Optimal Sizing of Battery Energy Storage Systems for Hybrid Marine Power Systems

Rene Barrera-Cardenas, Olve Mo and Giuseppe Guidi
Energy Systems, Sintef Energy Research, Trondheim, Norway
Rene.Barrera-Cardenas@sintef.no, olve.mo@sintef.no, giuseppe.guidi@sintef.no

***Abstract*—This paper introduces an analytical design methodology for Battery Energy Storage Systems (BESS) in hybrid marine vessels. Models for performance evaluation of a BESS composed by a battery array, an AC/DC power converter and a transformer are introduced and used to evaluate the potential fuel savings, projected lifetime and cost-benefit of BESS installation on a considered hybrid marine power system. By parametric sweep of free design parameters, the trade-off between different performance indices is analyzed and the optimal sizing (energy capacity and rated power) of the BESS can be obtained.**

Keywords— BESS sizing, BESS design, Hybrid Marine Power Systems, Hybrid Electric Vessel.

I. Introduction

Stricter regulations for marine vessels are undergoing like the introduction of maximum Energy Efficiency Design Index for new ships [1, 2] and the planned expansion of the current Emission Control Area in Europe [1], so there is a need for reducing fuel consumption and cut emissions in future Marine Power Systems (MPS). Normally, the vessel operation is restricted by rules, regulations and procedures for safety, so it is often not possible or allowed to operate diesel/gas generators at best efficiency [3]. Introducing an Energy Storage System (ESS) in MPS introduces an extra degree of freedom for the Energy Management System (EMS), which can be used to improve ship overall energy efficiency under different operation conditions, making the Hybrid-MPS (HMPS) an attractive solution for future marine vessels.

The choice of ESS technology is related to the ESS-technology's performance and functional requirements that best fits the area of application. An obvious application of ESS in HMPS is to serve as backup power source, which requires an ESS technology with high energy density and rate of discharge [4]. Many suitable ESS technologies are offered in the market Today. ESS based on battery technology have been successfully applied in road transportation [5, 6], resulting in major improvements of battery technology regarding key performance parameters like energy density, lifetime and safety. Volume production has also contributed to significant cost reduction [7, 6]. Therefore, a Battery Energy Storage System (BESS) can be considered as good alternative for Hybrid Marine Power Systems.

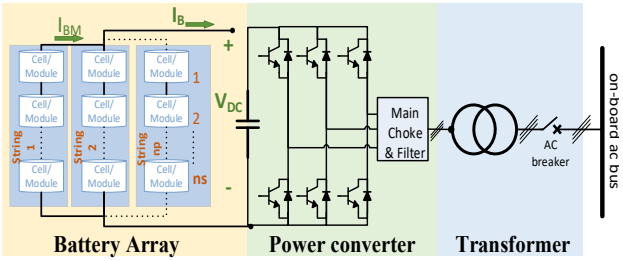

Fig. 1 Considered Battery Energy Storage System

This paper introduces a design methodology for optimal sizing of BESS in HMPS. The methodology explores the trade-off between different performance indices (potential fuel savings, projected BESS lifetime and cost-benefit index) by parametric sweep of free design parameters. The methodology is applied on a HMPS with onboard Diesel Generators (DGs) and BESS without charging from shore. However, the proposed methodology can be adapted to others HMPS, like 'plug-in' HMPS. As the use of BESS can contribute to increase HPMS performance in several different ways [8, 9], then two specific cases are considered to illustrate the proposed methodology: Strategic Loading (SL) and Spinning Reserve (SR) [3]. When BESS is used for SL, the operation point of DGs is shifted by cycling the BESS to minimize fuel consumption. In the SR case, the BESS is considered as part of the backup source in case of contingencies, so the number of running DGs could be reduced for optimal operation.

First, the models and parameters for evaluation of power losses, cost and lifetime of a battery energy storage system based on Li-ion battery technology are presented in section II. Then, the BESS design methodology is introduced in section III, where the BESS models are used to evaluate the HMPS performance. The results for BESS design solutions from a parametric sweep of considered free design parameters, are presented in section IV. Finally, main conclusions are summarized in section V.

II. Modelling of Battery Energy Storage Systems

A. BESS Topology

The considered BESS topology is shown in Fig. 1, and it is composed by a battery array, an AC/DC bidirectional power converter and a line transformer. The battery array consists of n_p parallel connected strings, each of them with n_s battery cell/modules series connected to fulfill the desired DC voltage (V_{DC}). The AC/DC power converter is assumed to be a two-level Voltage Source Converter (VSC), which is a

TABLE I. Characteritics for the considered Battery Module

Property	*Unit*	*Value*
Reference	Seanergy 48P from Saft	
Nominal Voltage (V_{be})	V	46.2
Nominal Energy at 0.2 C-rate	Wh	2600
Nominal Capacity at 0.2 C-rate	Ah	60
Maximum continuos currrent ($I_{bC.mx}$, $I_{bD.mx}$)	A	240 (Charge) 240 (Discharge)
Voltage Window	V	37.8 to 53.2
Equivalent Resistance (R_{be})	mΩ	16 (Charge) 12 (Discharge)
Nominal Energy Density	Wh/l	76

This is the accepted version of a paper published in 2019 IEEE Electric Ship Technologies Symposium - ESTS 2019
DOI: 10.1109/ESTS.2019.8847932

typical topology for interfacing the battery array and power flow control [8]. The transformer is typically used for insulation and to fit the voltage ratio to the main grid.

B. Considered Battery Module

The battery module Seanergy 48P, from Saft manufacturer [10], has been considered to illustrate the application of the proposed methodology. Table I shows the main characteristics of the considered battery module.

C. Power losses

The BESS power losses are estimated by

$$P_{l.BESS} = P_{Loss.B} + P_{Loss.VSC} + P_{Loss.TR} \quad (1)$$

where $P_{Loss.B}$ are the battery array losses, $P_{Loss.VSC}$ are the VSC losses and $P_{Loss.TR}$ are the transformer losses. The battery array losses can be estimated by

$$P_{Loss.B} = R_B \cdot I_B^2 = \frac{n_s}{n_P} \cdot R_{be} \cdot \frac{P^2}{V_{DC}^2} \quad (2)$$

where I_B is the total battery array current, R_{be} is the equivalent resistance of a single cell/module and P is the input/output power of the battery array. The value of R_{be} could be different for charge or discharge operation, so (2) can be used to estimate battery array losses in each operation by replacing the appropriated R_{be} value.

The VSC losses are mainly determined by the power semiconductors and the filter inductors, as filter capacitors losses are typically negligible for this topology [11]. Power semiconductor losses are calculated by the sum of conduction losses (P_{cond}) and switching losses (P_{sw}):

$$P_{Cond} = K_{cond0} \cdot P + K_{cond1} \cdot P^2 \quad (3)$$

$$P_{sw} = K_{sw} \cdot f_{sw} \cdot V_{DC} \cdot P \quad (4)$$

where f_{sw} is the switching frequency of the VSC, and K_{cond0}, K_{cond1} and K_{sw} are proportionally parameters which depends on converter operation (inverter or rectifier), modulation strategy and semiconductor module on-state and dynamic characteristics. Additionally, the semiconductor module is selected depending on VSC power rating and voltage class, making it hard to estimate the value for these loss parameters. In order to simplify the estimation of these parameters as function of the VSC power rating (P_N), the analysis presented in [11] is considered. Assuming a sinusoidal PWM modulation and a 1.7kV-class IGBT module technology, K_{cond0}, K_{cond1} and K_{sw} can be estimated by

$$K_{cond0} = \frac{6}{\pi \cdot V_{ac} \cdot PF} \quad (5)$$

$$K_{cond1} = \frac{6 \cdot \left(k_{a1T}^2 \cdot (k_{RT} - k_{RD}) + \frac{k_{RD}}{2}\right)}{\sqrt{6} \cdot k_{OF} \cdot V_{ac} \cdot PF \cdot P_N} \quad (6)$$

$$K_{sw} = \frac{2 \cdot \sqrt{6} \cdot K_E}{\pi \cdot V_{ac} \cdot PF} \quad (7)$$

where V_{ac} is the VSC line-to-line voltage, PF is the VSC power factor, k_{a1T} is the ratio of IGBT rms current to the VSC line current, k_{RT} and k_{RD} are the product of on-state resistances and nominal module current at 25°C for IGBT and diode, respectively, k_{OF} is the overrating factor for module selection and K_E is the total switching energy (Turn on, off and reverse recovery) per Ampere-Volt of the semiconductor module technology. The value of k_{a1T} depends on operation mode of VSC and it can be calculated as follows:

$$k_{a1T.D}^2 = 1 - k_{a1T.C}^2 = \frac{3 \cdot \pi + 8 \cdot M_{sN} \cdot PF}{12 \cdot \pi} \quad (8)$$

where $k_{a1T.D}$ is for inverter mode (when BESS is discharging), $k_{a1T.C}$ is for rectifier mode (when BESS is charging), and M_{sN} is the modulation index at nominal operating point.

TABLE II. POWER LOSS MODEL PARAMETERS

Parameter	*Value*	*Units*	*Parameter*	*Value*	*Units*
k_{RT}	1.4436	$\Omega \cdot A$	k_{RD}	0.8964	$\Omega \cdot A$
k_E	1.188	$\frac{\mu J}{V \cdot A}$	k_{OF}	1.8	--
M_{sN}	0.9	--	PF	1	--
δ_{iL}	0.1	--	α_L, β_L	1.1, 2	--
K_{VL0}	3.4353	dm^3	K_{VL1}	0.6865	--
K_{pw0}	9.412	kW	K_{pw1}	0.8536	--
K_{pc0}	8.242	kW	K_{pc1}	0.9993	--
$P_{TR.mn}$	0.005	--	f_1	50	Hz
$P_{TR.ref}$	0.02	--	$P_{N.ref}$	0.1	MW
Semiconductor Ref. Technology Infineon IGBT4 – 1.7kV			Inductor Ref. technology Siemens reactor series 4EUXX		

The filter inductor losses are composed by winding losses (P_{wL}) and core losses (P_{cL}). The winding losses can be calculated by using the equivalent winding resistance of the inductor (R_{wL}) and the core losses can be approximated by the empirical Steinmetz equation and assuming the peak flux density (B_L) to be proportional to the inductor current (I_L):

$$P_{wL} = R_{wL} \cdot I_L^2 = K_{wL} \cdot P^2 \quad (9)$$

$$P_{cL} = K_{core} \cdot f_L^{\alpha_L} \cdot B_L^{\beta_L} \cdot Vol_{core} = K_{cL} \cdot P^{\beta_L} \quad (10)$$

where K_{core}, α_L and β_L are the usual Steinmetz coefficient, and Vol_{core} is the inductor core. The analysis presented in [11] is used to estimate K_{wL} and K_{cL} as function of the VSC power rating, where winding and core losses at nominal power are calculated by:

$$P_{wL}(P_N) = K_{pw} \cdot (K_{VL0} \cdot (K_{LN} \cdot P_N)^{K_{VL1}})^{K_{pw1}} \quad (11)$$

$$P_{cL}(P_N) = K_{pc} \cdot (K_{VL0} \cdot (K_{LN} \cdot P_N)^{K_{VL1}})^{K_{pc1}} \quad (12)$$

$$K_{LN} = \frac{\left(1 - 3\sqrt{2} \cdot \frac{M_{sN}}{8}\right)}{3\sqrt{2} \cdot PF \cdot \delta_{iL} \cdot f_{sw}} \quad (13)$$

$$K_{pw} = K_{pw0} \cdot \left(1 + \left(\frac{2}{3} + \left(\frac{2f_{sw}}{\pi f_1}\right)^2\right) \cdot \left(\frac{\delta_{iL}^2}{6}\right)\right) \quad (14)$$

$$K_{pc} = K_{pc0} \cdot \left(\frac{\left(6 + \left(\delta_{iL} \cdot \frac{f_{sw}}{f_1}\right)^2\right)}{6 + \delta_{iL}^2}\right)^{\frac{\alpha_L}{2}} \cdot \left(1 + \frac{\delta_{iL}}{2}\right)^2 \quad (15)$$

where δ_{iL} is the ratio of peak-to-peak current ripple to maximum fundamental current, f_1 is the fundamental grid frequency and, K_{pwi}, K_{pci} and K_{VLi} ($i=0,1$) are proportionality regression coefficients found by taking data from reference

This is the accepted version of a paper published in 2019 IEEE Electric Ship Technologies Symposium - ESTS 2019
DOI: 10.1109/ESTS.2019.8847932

inductor technology for nominal winding losses versus volume, nominal core losses versus volume and volume versus energy relationships, respectively. Then, K_{wL} and K_{cL} can be evaluated by:

$$K_{wL} = \frac{Kpw \cdot \left(K_{VL0} \cdot {K_{LN}}^{K_{VL1}}\right)^{K_{pw1}}}{P_N^{\left(2-K_{VL1}\cdot K_{pw1}\right)}} \quad (16)$$

$$K_{cL} = \frac{Kpc \cdot \left(K_{VL0} \cdot {K_{LN}}^{K_{VL1}}\right)^{K_{pc1}}}{P_N^{\left(\beta_L-K_{VL1}\cdot K_{pc1}\right)}} \quad (17)$$

Finally, transformer losses are estimated by:

$$P_{Loss.TR} = K_{TR0} \cdot P_N + K_{TR1} \cdot P^2 \quad (18)$$

where K_{TR0} is the per unit transformer core losses and K_{TR1} is a proportionality constant related with the transformer winding losses. Normally for power transformers, the nominal transformer efficiency increases as transformer power rating increases, and by assuming that the core losses are equal to winding losses at nominal power, K_{TR0} and K_{TR1} can be estimated as follows:

$$K_{TR0} = K_{TR1} \cdot P_N = \frac{P_{TR.mn}}{2} + \frac{\left(P_{TR.ref} - P_{TR.mn}\right)P_{N.ref}}{2 \cdot P_N} \quad (19)$$

where $P_{TR.ref}$ is the reference transformer nominal loss in per unit, $P_{N.ref}$ is the reference transformer nominal power and $P_{TR.mn}$ is the minimum asymptotic transformer nominal loss in per unit. Table II list the power losses parameters used in this paper. Fig. 2 shows an example of BESS loss evaluation considering a fix switching frequency of 1600Hz, 800V DC voltage, the battery array composed by battery modules defined in Table I and the number of parallel strings selected to charge/discharge each battery module with 1 C-rate at nominal power.

D. BESS Cost

The BESS total investment cost (C_{BESS}) is calculated by adding the total battery array cost (C_{Bat}) and the total power electronics converter cost (C_{PEC}) including power transformer cost. The battery array cost is estimated based on model reported in [12]:

$$C_{Bat} = K_{Cost1} \cdot N_B + K_{Cost0} \quad (20)$$

where N_B is the total number of cell/modules ($N_B = n_p \cdot n_s$) and K_{Cost1}, K_{Cost0} are the cost per cell/module (618 [€]) and fix array cost constant (299.2 [€]), respectively. On the other hand, C_{PEC} is assumed to be proportional to the rated converter power ($C_{PEC} = K_{CPE} \cdot P_N$), with 100 [€/kW] as proportionality constant [13].

E. BESS lifetime

The lifetime estimation is a key aspect in the design of a BESS with high economic feasibility. The BESS lifetime is mainly limited by the battery cells. Aging process in battery cells is reflected mainly in capacity loss and increment of internal resistance. For Li-ion batteries, it has been found that capacity degradation provides a better end of life (EOL) criterion than the increase of cells internal resistance [13]. Thus, the EOL criterion (k_{EOL}) for BESS has been related to the capacity fade of battery cells:

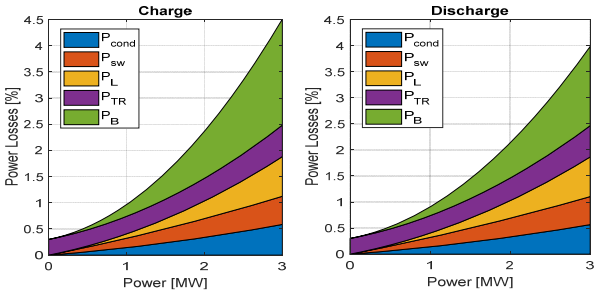

Fig. 2 Example of BESS Power Loss Evaluation as percentage of nominal power. Power Loss breakdown for a 3 MW BESS (left: charge, right: Discharge).

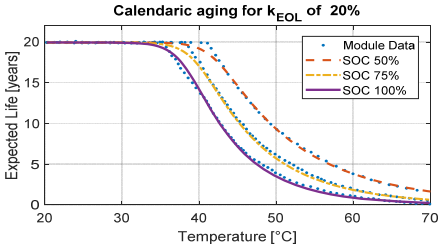

Fig. 3 Proposed calendar degradation model fitted for seanergy module data from Saft manufacturer

TABLE III. CALENDAR DEGRADATION FITTED PARAMETERS FOR THE SEANERGY BATTERY MODULE FROM SAFT.

α_c	k_{c1}	k_{c2}	k_{c3}	k_{c4}	k_{c5}
0.548	0.0054	18.77	-20173	-47513	-12.602

$$k_{EOL} = \left(1 - \frac{Q_{EOL}}{Q_{BOL}}\right) \cdot 100\% \quad (21)$$

where Q_{BOL} is the BESS total capacity at beginning of life and Q_{EOL} is the remain BESS capacity at end of life.

The estimation of the fractional capacity degradation (capacity fade in a period with defined conditions) depends on whether BESS is in operation (charging/discharging) or not. When the BESS is not in operation, the phenomena is known as calendar degradation (aging during storage). On the other hand, if the BESS is in operation, then a cycling degradation will occur.

Calendar degradation is influenced by cell temperature (T_{ce}) and idling State of Charge (SOC_0) [14]. It is proposed to estimate the fractional calendar degradation ($D_{Q.cal}$) in a period (Δt) as follows:

$$D_{Q.cal} = \left(1 - e^{-K_{cal}\cdot(t_0+\Delta t)^{\alpha_c}}\right) - \frac{Q_{loss}(t_0)}{Q_{BOL}} \quad (22)$$

$$K_{cal} \cdot t_0^{\alpha_c} = -\log\left(1 - \frac{Q_{loss}(t_0)}{Q_{BOL}}\right) \quad (23)$$

$$\log(K_{cal}) = \log(k_{cal0}) + \frac{k_{cal1}}{\left(1 + {k_{cal2}}^{200}\right)^{0.005}} \quad (24)$$

$$k_{cal0} = k_{c1} \cdot e^{k_{c2}\cdot SOC_0} \quad (25)$$

$$k_{cal1} \cdot R_g \cdot T_{ce} = (k_{c3} + k_{c4} \cdot SOC_0) \quad (26)$$

$$k_{cal2} = {k_{cal1}}\Big/{(k_{c5} - \log(k_{cal0}))} \quad (27)$$

where $Q_{loss}(t_0)$ is the capacity loss at beginning of period, R_g is the ideal gas constant (R_g=8.31446) and α_c, $k_{ci\ (i=1,\ldots5)}$ are

This is the accepted version of a paper published in 2019 IEEE Electric Ship Technologies Symposium - ESTS 2019
DOI: 10.1109/ESTS.2019.8847932

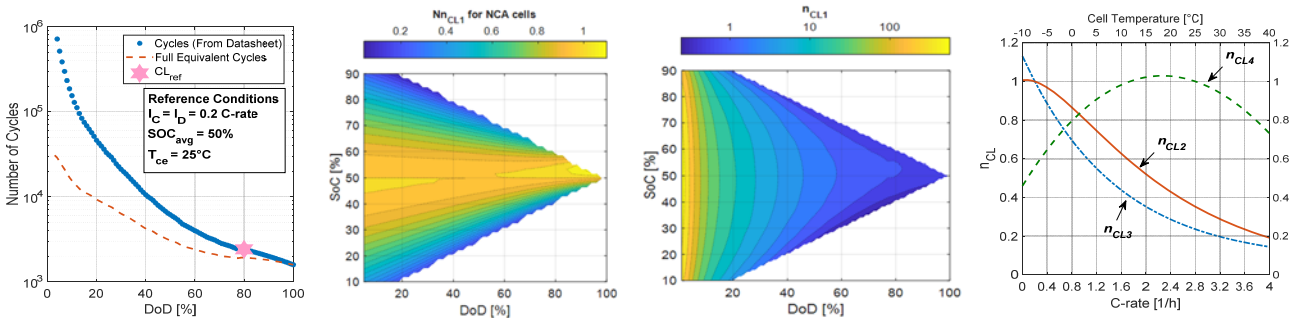

Fig. 4 Considered cycling degradation model fitted for seanergy module. (Left) Information from seanergy module datasheet; (middle left) normalized function Nn_{CL1} calculated from reference model [15] and assumed same for all NCA cells, (middle right) fitted n_{CL1} function based on seanergy module datasheet information ($n_{CL1}(DoD, 50\%)$) and Nn_{CL1} for NCA cells; and (right) fitted functions n_{CL2}, n_{CL3} *and* n_{CL4} for considered seanergy module.

fitting parameters of calendar degradation data provided by battery cell manufacturer, which are reported in Table III for the considered module. Fig. 3 shows calendar life data of Saft seanergy module (Table I) provided by manufacturer and the fitted model (22)-(27).

On the other hand, the multi-factor cycle life prediction methodology reported in [15] is used for estimation of fractional cycling degradation per cycle ($D_{Q.cyc}$), where the main assumption is that the impact of main operational factors on battery cycle life are approximated to be independent from each-other, and assuming that the cycling degradation is uniform distributed along the lifetime, it follows:

$$D_{Q.cyc} = \frac{0.01 \cdot k_{EOL.ref}/CL_{ref}}{n_{CL1}(DoD, SOC_{avg}) n_{CL2}(I_C) n_{CL3}(I_D) n_{CL4}(T_{ce})} \quad (28)$$

where DoD is the depth of discharge, SOC_{avg} is the average SOC during cycle, I_C and I_D are the charging and discharging currents, respectively, CL_{ref} is the number of cycles under reference conditions until the battery reaches its reference EOL criteria ($k_{EOL.ref}$) and n_{CLi} are the normalised cycle life functions, which are the battery cycle life under particular conditions divided by cycle life under reference conditions.

Normalised cycle life functions can be found in [15] as well as model fit parameters for a Panasonic NCA103450 battery cell. Since, one of the main limitations of applying model (28) to a given battery module, is the amount of data needed to fit the normalised functions, then, it has been assumed that battery cells with similar chemistry will have similar normalized functions.

Table IV shows and compares reference conditions for reference battery cell and assumed conditions for the considered battery module in this paper. For the considered Saft seanergy module, only the $CL(DoD)$ relationship at 50%

TABLE IV. REFERENCE CONDITIONS FOR CYCLING LIFE MODEL

Reference Conditions	*Panasonic NCA103450*	*Seanergy 48P module from Saft*
$k_{EOL.ref}$	20%	30%
CL_{ref}	650 cycles	2398 cycles
DoD	100 %	80 %
SOC_{avg}	50%	50%
T_{ce}	25°C	25°C
I_C	0.7 C-rate (max. 4 C-rate)	0.2 C-rate (max. 4 C-rate)
I_D	1 C-rate (max. 15 C-rate)	0.2 C-rate (max. 4 C-rate)

SOC_{avg} is reported in datasheet, so the other relationships are assumed to be like reported reference model parameters for NCA103450 battery cell, but adapted to seanergy module ratings, as both are Li-ion batteries with Nickel-Cobalt-Aluminium-Oxide (NCA) cathode. So, reported parameters for n_{CL2} and n_{CL3} have been scaled with maximum C-rate of the considered module, and n_{CL4} has been assumed same as reference model. Also, the ratio $Nn_{CL1} = n_{CL1}/n_{CL1}(DoD, 50\%)$ has been assumed to be the same for all cells with NCA cathode, so n_{CL1} is estimated by the product between Nn_{CL1} (calculated from reference model fo NCA cells) and $n_{CL1}(DoD, 50\%)$ (found in seanergy module datasheet). Fig. 4 shows the cycling degradation model fitted for seanergy modules as well as cycle life data found from datasheet.

Finally, the total degradation in a period, where BESS has been cycled N_{cycle} times at different conditions and the BESS has been inoperative N_{cal} intervals, can be calculated as follows:

$$\frac{Q_{loss}}{Q_{BOL}} = \sum_{i=1}^{N_{cal}} D_{Q.cal(i)} + \sum_{k=1}^{N_{cycle}} D_{Q.cyc(k)} < \frac{k_{EOL}}{100} \quad (29)$$

III. BESS DESIGN METHODOLOGY

A. *Hybrid Marine Power System and Reference Case*

The BESS design methodology proposed in this paper is applied to the HMPS shown in Fig. 5, consisting of two AC power bus bars, a BESS and four identical Diesel Generators (DGs), which supply the propulsion and hotel loads. A multi-objective design approach is adopted and the performance indices of the HMPS are compared against a reference case, a marine power system with similar architecture as HMPS in Fig. 5, but without BESS. So, potential benefits of adding BESS to existing marine vessel can also be analysed by the propose methodology.

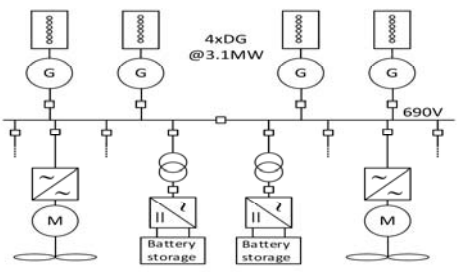

Fig. 5 Considered Hybrid Marine Power System

This is the accepted version of a paper published in 2019 IEEE Electric Ship Technologies Symposium - ESTS 2019
DOI: 10.1109/ESTS.2019.8847932

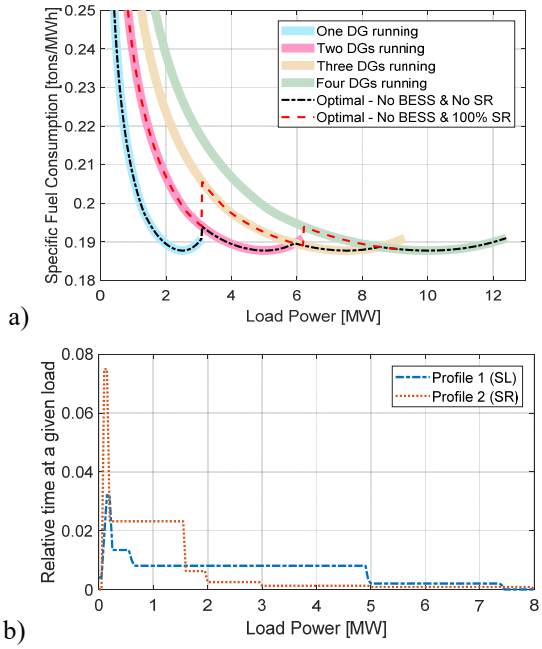

Fig. 6 Considered Inputs for fuel consumption estimation: a)SFC for 1-4 DGs running (including optimal SFC for reference case with and without SR), b) Load probability distribution for profile 1 (operation under SL) and profile 2 (operation with required SR).

HMPS performance depends on the selected/designed Energy Management Strategy (EMS) for a given operating mode of the marine vessel. Different operating modes (e.g. dynamic positioning, roll-on/roll-off operation, or offshore petroleum discharge) can be considered by associating them to a load profile and operating constraints, so the total performance can be estimated by weighted average considering the relative time that the vessel is at each operation mode.

To illustrate the methodology, two generic load profiles are considered, which are focused on two different aspects: Strategic Loading (SL) and Spinning Reserve (SR). EMS for SL uses the BESS to minimize fuel consumption by shifting the operation point of DGs. On the other hand, BESS used as SR refers to the use of BESS as backup source in case of contingencies, so the HMPS can be operated with optimal number of running DGs while still fulfilling the redundancy requirements. It is assumed that when the system is operated in SL, then SR is not required, and vice versa.

The analytical method reported in [3] for estimation of fuel savings potential resulting from installation of BESS in marine vessels, is considered in this paper. To estimate the fuel consumption, the methodology basically requires two inputs, the Specific Fuel Consumption (SFC) of the DGs and the load probability distributions of the considered load profiles. Fig. 6a shows the considered SFC for DGs, when 1-4 DGs are running. It is also shown in Fig. 6a, the minimum achievable SFCs for reference case (system without BESS), assuming no required SR ($SFC_{DG,NSR}$) and 100% required SR ($SFC_{DG,SR}$ for P_{SR}=P_L):

$$SFC_{DG,NSR}(P_L) = \min_{n_{DG}}[SFC_{DG}(n_{DG}, P_L)] \tag{30}$$

$$SFC_{DG,SR}(P_L) = \min_{n_{DG}}[SFC_{DG}(n_{DG}, P_L)]$$
$$subject\ to\ (n_{DG} - 1) \cdot P_{DG.mx} \geq P_{SR} \geq P_L \tag{31}$$

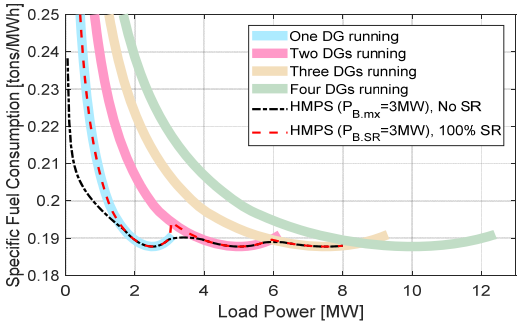

Fig. 7 Example of SFC of HMPS for operation under SL and operation with 100% SR, when the BESS has a maximum power capability of 3MW

where n_{DG} is the number of running DGs, P_L is the load power, $P_{DG.mx}$ is the DG rated power, and P_{SR} is the required SR. On the other hand, Fig. 6b shows the load probability distribution for profile 1 ($F_{pd.NSR}$: operation under SL and without SR) and profile 2 ($F_{pd.SR}$: operation with required SR but no SL). It is also considered that for an annual operation, the vessel is operating under profile 1 for six months, and the remaining time the vessel operates with profile 2.

B. *Energy Management Strategy for HMPS*

The EMS for minimum fuel consumption in SL and SR operations, reported in [3], is considered for HMPS fuel consumption estimation. The SFC for HMPS operating under SL ($SFC_{HMPS,NSR}$), is estimated by

$$SFC_{HMPS,NSR}(P_L) = \min_{n_C, n_D, P_{BC}, P_{BD}}[SFC_{SL}]$$
$$subject\ to \left\{ \begin{array}{c} 0 \leq P_{BC} \leq P_{BC.mx} \\ 0 \leq P_{BD} \leq P_{BD.mx} \\ 0 \leq n_D \leq 4 \\ n_D \leq n_C \leq 4, \quad n_C > 0 \end{array} \right\} \tag{32}$$

where n_C and n_D are the number of running DGs during charge and discharge, respectively, P_{BC} and P_{BD} are the charging and discharging power, respectively, and SFC_{SL} is the equivalent SFC taking the battery cycling into account:

$$SFC_{SL} = \frac{SFC_{DG}(n_c, P_L + P_{BC})}{k_{TC}} + \frac{SFC_{DG}(n_D, P_L + P_{BD})}{k_{TD}}$$
$$k_{TC} = \frac{P_{BC} + P_{BD} - P_{l.BESS,C} + P_{l.BESS,D}}{P_{BD} + P_{l.BESS,D}} \tag{33}$$
$$k_{TD} = \frac{P_{BC} + P_{BD} - P_{l.BESS,C} + P_{l.BESS,D}}{P_{BC} - P_{l.BESS,C}}$$

where $P_{l.BESS,C}$ and $P_{l.BESS,D}$ are the BESS losses while charging and discharging, respectively. On the other hand, the SFC for HMPS operating with required SR ($SFC_{HMPS,SR}$), is estimated by:

$$SFC_{HMPS,SR}(P_L) = \min_{n_{DG}}[SFC_{DG}(n_{DG}, P_L)]$$
$$suject\ to\ (n_{DG} - 1) \cdot P_{DG.mx} \geq P_{SR} - P_{B,SR} \tag{34}$$

where $P_{B,SR}$ is the maximum reserved power capacity of BESS for SR. Fig. 7 shows an example of SFC of HMPS for operation under SL and operation with 100% SR, when the BESS has a maximum power capability of 3MW ($P_{BC.mx} = P_{BD.mx} = P_{B,SR} = 3MW$).

This is the accepted version of a paper published in 2019 IEEE Electric Ship Technologies Symposium - ESTS 2019
DOI: 10.1109/ESTS.2019.8847932

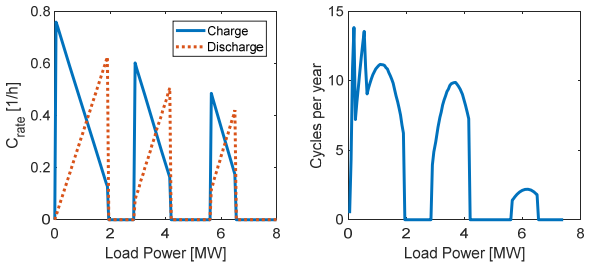

Fig. 8 Example of cycling stress profiles and estimated number of cycles per year for the load profile 1 shown in Fig. 6-b, and when $E_{BN} = 3MWh$, $P_N = 3MW$, $DoD_{MX} = 60\%$

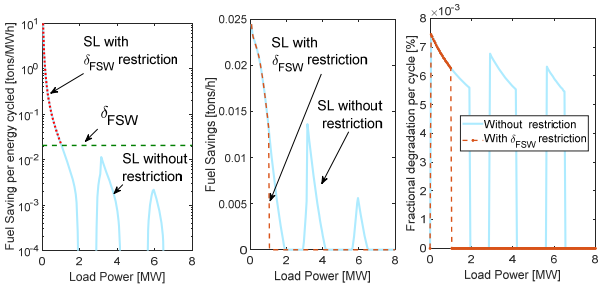

Fig. 9 Example of how the threshold value for minimum fuel savings per MWh throughput modifiy fuel savings and cycling degradation for the load profile 1 shown in Fig. 6-b, when $E_{BN} = 3MWh$, $P_N = 3MW$, $DoD_{MX} = 60\%$

C. Free Design parameters and constants

First, the number of battery cells/modules ($n_s \cdot n_p$) is directly linked to the desired nominal battery array voltage (V_{BN}) and nominal BESS energy capacity (W_{BN}) by

$$n_s = \frac{V_{BN}}{V_{be}} \qquad n_p = \frac{W_{BN}}{n_s \cdot W_{be}} \tag{35}$$

where V_{be} is the nominal voltage of the considered cell/module and W_{be} is the nominal energy per cell/module. The converter rated power (P_N) is freely selected within a predefined range but lower than the maximum battery array power capacity at EOL:

$$P_N \leq n_p \cdot V_{BN} \cdot \left(1 - \frac{k_{EOL}}{100}\right) \cdot \max\{I_{bC.mx}, I_{bD.mx}\} \tag{36}$$

where $I_{C.mx}$ and $I_{D.mx}$ are the maximum continuous current for charging and discharging, respectively. Then, the maximum charging and discharging power for HMPS operating under SL, which are needed to calculate EMS in (32), can be defined by:

$$P_{BC.mx} = \min\{\mathrm{P_N}, \quad n_p V_{BN} \cdot I_{bC.mx}\left(1 - \frac{k_{EOL}}{100}\right)\} \tag{37}$$

$$P_{BD.mx} = \min\{\mathrm{P_N}, \quad n_p V_{BN} \cdot I_{bD.mx}\left(1 - \frac{k_{EOL}}{100}\right)\} \tag{38}$$

Also, the maximum reserved power capacity of BESS for SR is estimated by:

$$P_{B,SR} = \frac{W_{BN} \cdot \left(1 - \frac{k_{EOL}}{100}\right)(SoC_{SR} - SoC_{mn})}{100 \cdot T_{SR}} - P_{l.BESS.D} \tag{39}$$

$$P_{B,SR} \leq P_N$$

where SoC_{SR} is the SoC of BESS while vessel is under SR operation (BESS is not cycled), SoC_{mn} is the SoC for cut-off discharging in case BESS should provide the SR, T_{SR} is the minimum time that BESS must keep providing the Spinning Reserve, and $P_{l.BESS.D}$ is the BESS power losses during discharge operation at rated power.

TABLE V. FREE DESIGN PARAMETERS AND CONSTANTS

$V_{BN}[V]$	{700, 1050}	$k_{t.NSR}$	0.5
$W_{BN}[MWh]$	{0.1, 6}	$T_{SR}[h]$	0.25
$P_N[MW]$	{0.25, 5}	$SOC_{SR}[\%]$	90
$k_{SL}[\%]$	{0, 100}	$SOC_{mn}[\%]$	10
$DoD_{MX}[\%]$	{10, 60}	$SOC_{avg}[\%]$	50
$k_{EOL}[\%]$	20	$f_{sw}[Hz]$	1600
$i_{rate}[\%]$	5	$K_{CF}[€/ton]$	1400
$T_{ce}[°C]$	30	$K_{CSS}[€]$	0.26 [16]

On the other hand, when HMPS is under SL operation, the maximum cycle duration at a given P_L can be estimated by:

$$T_{cycle} = E_{BN} \cdot \frac{DoD_{MX}}{100} \cdot \left(\frac{1}{P_{BC}(P_L)} + \frac{1}{P_{BD}(P_L)}\right) \tag{40}$$

where DoD_{MX} is the maximum allowed DoD under cycling in percentage. Then, by assuming that the load stays at a given P_L for long time, the number of cycles (N_{cycle}) per year can be roughly estimated by

$$N_{cycle} = \frac{8760 \cdot k_{t.NSR} \cdot \mathrm{Fpd_{NSR}}(P_L)}{T_{cycle}(P_L)} \tag{41}$$

where $k_{t.NSR}$ is the relative time per year the vessel is under SL operation, and $\mathrm{Fpd_{NSR}}$ is the load probability distribution for SL operation. Fig. 8 shows an example of cycling stress profiles, when $E_{BN} = 3MWh$, $P_N = 3MW$, and $DoD_{MX} = 60\%$.

Additionally, the EMS for SL operation (32) could be modified to prioritize energy cycling for load levels that give the largest payback in terms of fuel saving, as it is proposed in [3], so an additional trade-off between cycling degradation and fuel savings could be explored. Then, a threshold value for minimum fuel savings per MWh throughput (δ_{FSW}) is defined by

$$\delta_{FSW} = \frac{k_{SL}}{100} \cdot \max\left\{\frac{\left(SFC_{DG,NSR} - SFC_{HMPS,NSR}\right)}{\frac{E_{BN} \cdot DoD_{MX}}{100 \cdot T_{cycle}}}\right\} \tag{42}$$

where the term within {} is the fuel savings per MWh energy cycled through the BESS when SL strategy is used, and k_{SL} is a free design parameter in percentage between 0 and 100%, such that no additional restriction is considered for SL operation when $k_{SL} = 0$, and not SL operation at all is considered for $k_{SL} = 100\%$. Fig. 9 shows an example of how the threshold value for minimum fuel savings per MWh throughput modify fuel savings and cycling degradation, when $E_{BN} = 3MWh$, $P_N = 3MW$, and $DoD_{MX} = 60\%$.

Table V summarises the free design parameters and design constants considered in this study.

D. Performance Evaluation

In this study, the annual fuel savings (ΔFC), the projected lifetime (t_{EOL}) and the cost-benefit index (CBI) are the

This is the accepted version of a paper published in 2019 IEEE Electric Ship Technologies Symposium - ESTS 2019
DOI: 10.1109/ESTS.2019.8847932

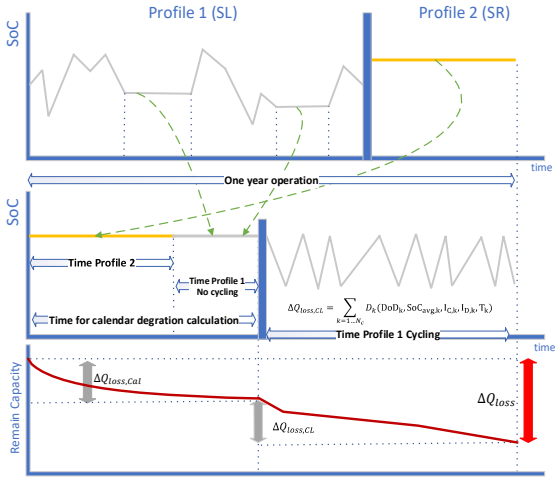

Fig. 10 Annual degradation calculation methodology.

considered performance indices. The annual fuel savings can be estimated by:

$$\Delta FC = 8760 \cdot (k_{t.NSR} \cdot \Delta FC_{NSR} + (1 - k_{t.NSR}) \cdot \Delta FC_{SR}) \quad (43)$$

$$\Delta FC_{NSR} = \int \mathrm{Fpd}_{\mathrm{NSR}} \cdot P_L \cdot (SFC_{DG,NSR} - SFC_{HMPS,NSR}) \cdot dP_L \quad (44)$$

$$\Delta FC_{SR} = \int \mathrm{Fpd}_{\mathrm{SR}} \cdot P_L \cdot (SFC_{DG,SR} - SFC_{HMPS,SR}) \cdot dP_L \quad (45)$$

On the other hand, the CBI is defined by

$$CBI = CFS_T - C_{BESS} - C_{SS} \quad (46)$$

$$CFS_T = \sum_{k=1}^{t_{EOL}} \frac{K_{CF} \cdot \Delta FC_k}{(1 + i_{rate})^k} \quad (47)$$

$$C_{BESS} = C_{bat} + C_{PEC} \quad (48)$$

$$C_{SS} = \sum_{k=1}^{t_{EOL}} \frac{K_{CSS} \cdot N_{SS}}{(1 + i_{rate})^k} \quad (49)$$

where CFS_T is the total present value benefit from fuel savings in t_{EOL} years, K_{CF} is the fuel cost per unit volume, C_{BESS} is the EBSS installation cost, C_{SS} is the associated cost of DGs Start&Stops during SL, K_{CSS} is the DG start-up cost, N_{SS} is the number of DG Start&Stops actions per year because SL operation ($N_{SS} \approx \sum N_{cycle}$.), and i_{rate} is the interes rate for present value calculation. The values for the cost constants are shown in Table V.

For lifetime estimation, the degradation calculations are based on quasi steady state approach but not considering load time series. An illustrative chart of annual degradation calculation methodology is shown in Fig. 10. The calendar degradation per year is calculated by assuming that all time BESS is inoperative (not cycling), has been consecutive (N_{cal} =1) and at the beginning of the year. On the other hand, the calculation of cycling degradation per year assumes that all cycling operations are consecutive as well as that cycles with same stress profiles have been consecutives. Micro-cycles are neglected. The projected lifetime (t_{EOL}) is obtained by repeat the annual degradation calculation with updated remain capacity until EOL criteria is reached.

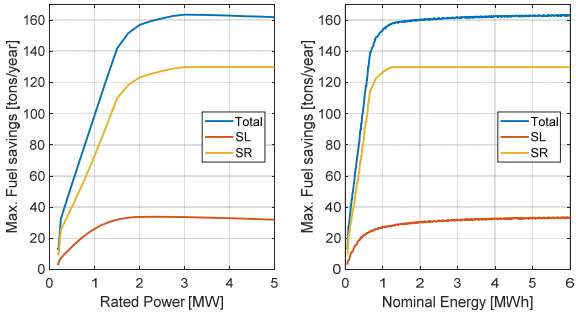

Fig. 11 Maximum Fuel Savings as function of (left) BESS Rated Power and (right) BESS Nominal Energy.

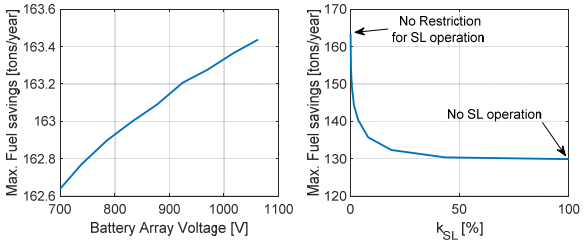

Fig. 12 Maximum Fuel Savings as function of: (left) BESS DC Voltage, and (right) the threshold factor for minimum fuel savings per MWh throughput in SL operation.

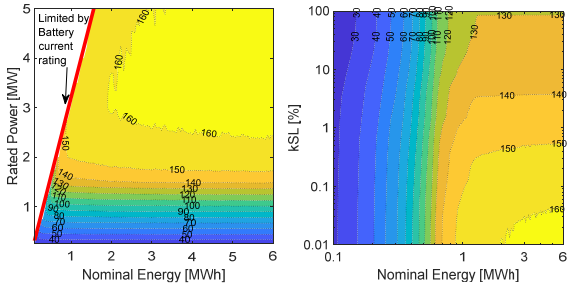

Fig. 13 Maximum Fuel Savings contour plot. (Left)Nominal energy vs Rated Power; (right) Nominal energy vs k_{SL}.

IV. Results

A. Fuel savings

Fig. 11 shows the solutions with maximum fuel savings as function of BESS Rated Power (left) and BESS Nominal Energy (right). From Fig. 11-left, it can be observed that there is an optimal value for P_N, around 3MW, which maximizes the total fuel savings to around 163.4 tons per year. On the other hand, it can be noted from Fig. 11-right that total fuel savings are proportional to nominal energy, reaching the maximum fuel savings for 6MWh nominal energy installed. However, it should be said that for nominal energy beyond 2 MWh, the curve has very low slope, increasing around 1.3 tons per year per each additional MWh installed.

The fuel savings components from SL and SR operation are also included in Fig. 11. It can be noted that most of the fuel savings are coming from SR operation. Also, fuel savings from SR reaches its maximum around 3.1 MW rated power and 1.25 MWh nominal energy. Beyond that point, no additional fuel savings from SR operation can be obtained. On the other hand, fuel savings from SL operation reaches its maximum for around 2.5 MW rated power and 6 MWh nominal energy. However, it can be noted that installing

This is the accepted version of a paper published in 2019 IEEE Electric Ship Technologies Symposium - ESTS 2019
DOI: 10.1109/ESTS.2019.8847932

capacity beyond 2 MWh has marginal improvement on fuel savings.

Fig. 12 shows the maximum fuel savings as function of BESS DC Voltage and k_{SL}. Regarding nominal battery array voltage, maximum fuel savings increases as voltage increases, as it can be observed from Fig. 12-left, but it can be noted that voltage influence on maximum fuel savings is negligible, so more than 162.5 tons per year can be obtained for any of the considered nominal voltages. On the other hand, it can be observed from Fig. 12-right that the maximum fuel savings decreases as k_{SL} increases. Since increments on k_{SL} are reflected on a more restrictive SL operation, then maximum fuel savings are reduced to only the maximum fuel savings from SR operation (around 130 tons/year) when $k_{SL} = 100\%$. It can be also noted that the fuel savings coming from SL operation are mainly for $k_{SL} < 40\%$, and the curve shows an exponential dependency on total fuel savings against k_{SL}. Additionally, it should be said that the maximum allowed DoD under cycling has not influence on the potential fuel savings, as this parameter only determines the stress on battery cells but not the power extracted from them.

It should be noted that Fig. 11 and Fig. 12 show maximum fuel savings as function of given parameters when all other parameters have been optimally selected. To explore the correlation between the design parameters and total fuel savings, Fig. 13 shows the total fuel savings contour plot for E_{BN} versus P_N (Fig. 13-left) and for E_{BN} versus k_{SL} (Fig. 13-right). It can be noted that by sizing the BESS to 2 MWh nominal energy and 3 MW rated power, a total fuel savings of 160 tons per year can be obtained, so almost no benefits in fuel savings will be obtained by increasing the BESS size beyond that design point. Also, it can be noted from Fig. 13-left that the contour lines are almost horizontals, which means that for a given value of P_N increments on E_{BN} will not have effect on fuel savings but for constant E_{BN}, the total fuel savings increases as P_N increases, so total fuel savings are strongly limited by P_N but not by E_{BN}. Additionally, it can be observed, from Fig. 13-right, that k_{SL} has low impact on fuel savings for E_{BN} lower than 0.8 MWh, as most of the fuel savings are coming from SR operation when small BESS is installed. However, for E_{BN} beyond 1.2 MWh the total fuel savings decreases as k_{SL} increases, but decrement is limited to maximum 18% (30 tons/year) of maximum fuel savings, which represent the fuel savings coming from SL operation.

B. *Cost-Benefit Index*

Fig. 14 shows the maximum Cost-Benefit Index as function of P_N and E_{BN} (top); DoD_{MX} and k_{SL} (middle); and V_{BN} (bottom). A maximum CBI value of 1.8 M€ is obtained for $P_N \approx 2$ MW, $E_{BN} \approx 0.83$ MWh, DoD_{MX} =10%, k_{SL} = 20% and V_{BN} = 693V (or 924V). It can be observed from Fig. 14-top that the CBI reduces with a slope of -0.225 M€/MWh for nominal energy beyond 1 MWh, and with -0.15 M€/MW for rated power beyond 2MW. Increment on BESS sizing beyond the optimal drastically reduces cost-benefit index with strongest dependency on E_{BN} than P_N, which can be explained from the higher cost of the battery modules than power electronics converter equipment, as an increment on E_{BN} directly implies more number of battery modules but an increment on P_N could be fulfilled by only increasing power converter size but keeping same number of battery modules operated at higher current stress and reducing BESS lifetime.

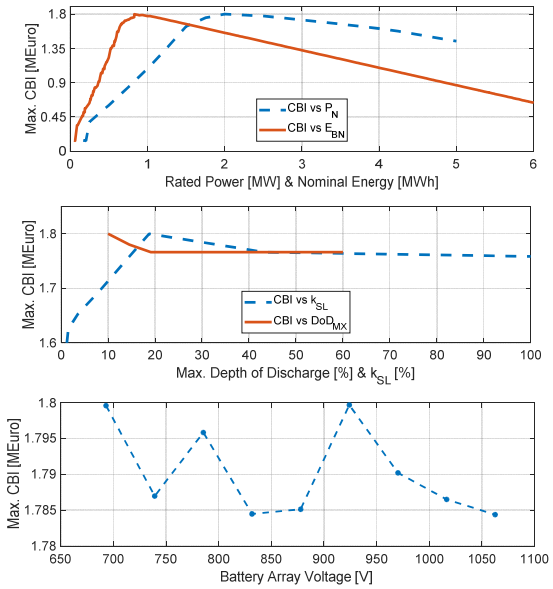

Fig. 14 Maximum Cost-Benefit Index as function of BESS Rated Power and BESS Nominal Energy (top),.maximum DoD and k_{SL} (middle), and Battery array voltage (bottom).

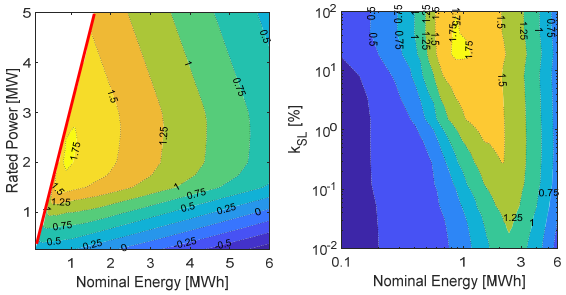

Fig. 15 Maximum Cost-Benefit Index contour plot. (left) Nominal Energy vs Rated power, (right) Nominal energy vs k_{SL}.

On the other hand, it can also be noted from Fig. 14 that variations of the others free design parameters (DoD_{MX}, V_{BN} and k_{SL}) from their optimal values have less impact on CBI (around 2% reduction from its maximum value), with the exception of very low values of k_{SL} (no restricted SL operation), as it drastically reduces BESS lifetime and therefore CBI value reduces even if fuel saving could be increased from the no restricted SL operation.

Fig. 15 shows the maximum CBI contour plot for E_{BN} versus P_N (Fig. 15-left), and E_{BN} versus k_{SL} (Fig. 15-right), so, the correlation between these design parameters and CBI can be explored. Compared with fuel savings (Fig. 13-left), CBI shows an optimal region smaller than the fuel savings case, so CBI is more sensible to small variations on BESS sizing. Also, from Fig. 15-left, it can be observed that for P_N lower than around 2 MW, increments on E_{BN} will require increment on P_N to keep the same CBI value, however, for P_N higher than 2 MW, any increment on E_{BN} will decreases CBI independently on P_N.

It can be also noted that optimal solutions are near to the limit of battery current rating (red line in Fig. 15-left), which can be explained because the major benefit is coming from fuel savings in SR operation where BESS is not cycling and only calendar degradation has been assumed to happened (independently on possible current stress in case of fault),

This is the accepted version of a paper published in 2019 IEEE Electric Ship Technologies Symposium - ESTS 2019
DOI: 10.1109/ESTS.2019.8847932

therefore the highest CBI is obtained by maximize the available spinning reserve power from the BESS.

Additionally, it can be observed from Fig. 15-right that for a given E_{BN} the SL operation should be always restricted ($15\% < k_{SL} < 40\%$) to maximize CBI and decreasing k_{SL} value will requires increment on E_{BN} to keep similar CBI values.

C. *Performance trade-off*

Fig. 16 shows the performance indices trade-off (Fuel Savings vs. CBI vs. Lifetime) for the considered BESS design. It can be noted that solutions with the highest CBI has lower Fuel Savings but the longest BESS Lifetime (around 20 years). The solutions with long BESS lifetime are linked to highly restricted SL operation, so BESS aging is mainly coming from calendar degradation. It can be noted that fuel savings and CBI are two conflicting objectives. The $\Delta FC - CBI$ trade-off (Pareto optimality) is also included in Fig. 16. The maximum CBI of 1.8 M€ is obtained for a fuel savings of about 125 tons/year, and the maximum fuel savings of 163.4 tons/year is obtained for a CBI value of 0.294 M€. Two different slopes in the Pareto optimality curve can be noted, a decrement of 11.8 k€ from maximum CBI per each ton/year of increment in fuel savings (from left to right in Fig. 16), and an increment of 432.4 k€ per each ton/year of decrement in fuel savings from its maximum (from bottom to top in Fig. 16). Trying to reach total fuel savings higher than 160 tons/years will affects drastically the CBI. Also, The Pareto optimality curve shows a clear intersection point (knee) where curve changes from one slope to the other and near that point the solutions have the best trade-off between Fuel savings and CBI.

Fig. 17 shows the free design parameters (E_{BN}, P_N, DoD_{MX} and k_{SL}) and performance indices (CBI and t_{EOL}) correlation for $\Delta FC - CBI$ Pareto-optimality trajectory (going from left to right in Fig. 16). The curves can be grouped in four segments along total fuel saving axis, as it can be noted from Fig. 17. As fuel savings is prioritized against CBI (from left to right), first (segment $125 < \Delta FC < 130$), BESS size (E_{BN}, P_N) is increased as well as DoD_{MX}. Then, to get total fuel savings beyond 130 tons/year, a less restrictive SL operation is needed and a second group of solutions can be distinguished from Fig. 17 (segment $130 < \Delta FC < 148$), where k_{SL} value decreases as fuel saving increases as well as BESS size (E_{BN}, P_N) keeps increasing but DoD_{MX} decreases in order to prolong lifetime and maximize CBI. Once P_N reaches its optimal value for maximize fuel savings (around 3 MW), then a third group of solutions can be observed (segment $148 < \Delta FC < 160$), where P_N and DoD_{MX} keep constant around 3 MW and 10%, respectively, while fuel savings increases by increasing E_{BN} and decreasing k_{SL} value until reach zero (No any restriction on SL operation). Finally, in order to get total fuel savings beyond 160 tons/year, E_{BN} needs to be increased with a very high slope of about 1.46 MWh per each tons/year fuel savings increment, also DoD_{MX} needs to be increased quickly in order to slow down the reduction on CBI by reducing the number of DG Start&Stops actions per year from SL operation.

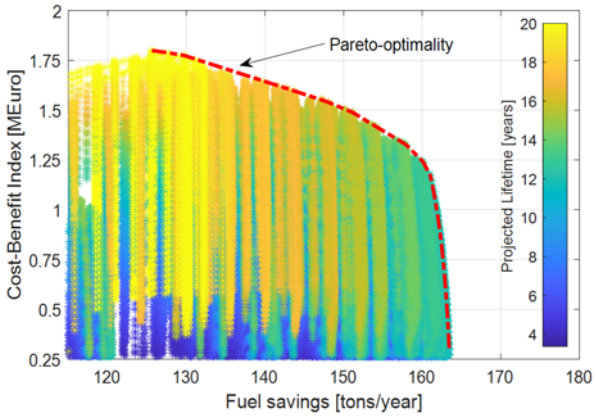

Fig. 16 Performance space: Cost-Benefit Index vs Fuel Savings vs Lifetime. $\Delta FC - CBI$ Pareto-optimality curve also included (red line).

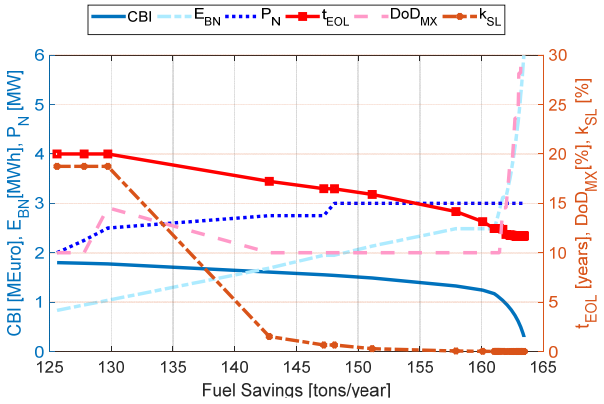

Fig. 17 Free design parameters and performance indices correlation for Pareto-optimality trajectory.

V. Conclusion

A BESS sizing methodology for hybrid marine power systems has been proposed and applied to a case-study with two distinctive operation profiles regarding if the BESS is used as spinning reserve source or not. The methodology proposes to evaluate the multidimensional performance space for a set of free design parameters by parametric sweeping. Three performance indices are used to evaluate and compare the BESS design space solutions: annual fuel savings, expected batteries lifetime and cost-benefit index. And the trade-off between the performance indices has been studied. By applying the proposed methodology, it was found that maximum fuel savings and CBI could be two conflicting objectives, so only a reduction on the potential fuel savings allows to increase the cost-benefit index.

In the considered case-study, it can be noted that CBI is proportional to BESS lifetime but not to BESS sizing, showing that it is more cost effective to install a moderate size BESS and optimize its use (by restricting SL operation and using it as spinning reserve source with high power capacity to energy capacity ratio), than increasing fuel savings by implementation of strategic loading and install a big sized BESS expecting to reduce cycling stress expecting to enlarge lifetime.

Performance evaluation strongly depends on operative mode and adopted energy management strategy. For the considered HMPS and load profiles, the most benefits are coming from the use of BESS as spinning reserve source. About 80 % of maximum possible fuel savings, the maximum CBI value and longest BESS lifetime are obtained for BESS used only as spinning reserve. Introducing strategic loading operation when not spinning reserve in required will increase total fuel saving while decreasing CBI and reducing BESS lifetime. Therefore, the use of BESS for strategic loading in HMPS need to be restricted. However, only fuel cost has been

This is the accepted version of a paper published in 2019 IEEE Electric Ship Technologies Symposium - ESTS 2019
DOI: 10.1109/ESTS.2019.8847932

considered in CBI definition as potential benefit from fuel savings, but additional benefits from fuel savings like economical incentives coming from governmental policies could make more convenient the implementation of BESS for strategic loading.

ACKNOWLEDGMENT

This paper present results from NFR project New Energy Storage Systems funded by The Research Council of Norway, project number 269490/E20.

REFERENCES

[1] International Maritime Organisation (IMO), "MARPOL Annex VI and NTC 2008 with Guidelines for Implementation," International Maritime Organisation (IMO), 2013.

[2] International Maritime Organisation (IMO), "Module 2 – Ship Energy Efficiency Regulations and Related Guidelines," in *IMO Train the Trainer (TTT) Course on Energy Efficient Ship Operation*, London, International Maritime Organisation, 2016, p. 45.

[3] O. Mo and G. Guidi, "Design of Minimum Fuel Consumption Energy Management Strategy for Hybrid Marine Vessels with Multiple Diesel Engine Generators and Energy Storage," in *2018 IEEE Transportation Electrification Conference and Expo (ITEC)*, Long Beach, CA, USA, 2018.

[4] E. Skjong, R. Volden, E. Rødskar, M. Molinas, T. A. Johansen and J. Cunningham, "Past, Present, and Future Challenges of the Marine Vessel's Electrical Power System," *EEE Transactions on Transportation Electrification,* vol. 2, no. 4, pp. 522-537, 2016.

[5] S. Alahakoon and M. Leksell, "Emerging Energy Storage Solutions for Transportation – A Review: An Insight into Road, Rail, Sea and Air Transportation Applications," in *2015 International Conference on Electrical Systems for Aircraft, Railway, Ship Propulsion and Road Vehicles (ESARS)*, Aachen, Germany, 2015.

[6] S. M. Lukic, J. Cao, R. C. Bansal, F. Rodriguez and A. Emadi, "Energy Storage Systems for Automotive Applications," *IEEE Transactions on Industrial Electronics,* vol. 55, no. 6, pp. 2258 - 2267, 2008.

[7] B. Sarlioglu, C. T. Morris, D. Han and S. Li, "Driving Toward Accessibility: A Review of Technological Improvements for Electric Machines, Power Electronics, and Batteries for Electric and Hybrid Vehicles," *IEEE Industry Applications Magazine,* vol. 23, no. 1, pp. 14-25, 2017.

[8] D. Radan, M. Southall, M. Benatmane and M. Butcher, "Integration, optimisation and benefits of energy storage for marine applications," in *2016 International Naval Engineering Conference (INEC).*, 2016, 2016.

[9] Z. Zhou, M. Benbouzid, J. F. Charpentier, F. Scuiller and T. Tang, "A review of energy storage technologies for marine current energy systems," *Renewable and Sustainable Energy Reviews,* vol. 18, pp. 390-400, 2013.

[10] Saft, "Seanergy module - Datasheet," June 2017. [Online]. Available: https://www.saftbatteries.com. [Accessed 16 03 2019].

[11] R. A. Barrera-Cardenas, Meta-parametrised meta-modelling approach for optimal design of power electronics conversion systems: Application to offshore wind energy, Trondheim, Norway: PhD Thesis, NTNU, 2015.

[12] TIAX LLC, "Cost Assessment for Plug-In Hybrid Vehicles (SOW-4656)," Report to the US DOE Office of Transportation Technology, 2007.

[13] M. Swierczynski, D.-I. Stroe, A.-I. Stan and R. Teodorescu, "Lifetime and economic analyses of lithium-ion batteries for balancing wind power forecast error," *INTERNATIONAL JOURNAL OF ENERGY RESEARCH,* vol. 39, pp. 760-770, 2015.

[14] S. Grolleau, A. Delaille, H. Gualous, P. Gyan, R. Revel, J. Bernard, E. Redondo-Iglesias and J. Peter, "Calendar aging of commercial graphite/LiFePO4 cell - Predicting capacity fade under time dependent storage conditions," *Journal of Power Sources,* vol. 255, pp. 450-458, 2013.

[15] V. Muenzel, J. d. Hoog, M. Brazil, A. Vishwanath and S. Kalyanaraman, "A Multi-Factor Battery Cycle Life Prediction Methodology for Optimal Battery Management," in *2015 ACM Sixth International Conference on Future Energy Systems*, Bangalore, India, 2015.

[16] C. Liu, X. Wang, X. Wu and J. Guo, "Economic scheduling model of microgrid considering the lifetime of batteries," *IET Generation, Transmission & Distribution,* vol. 11, no. 3, pp. 759-767, 2017.

This is the accepted version of a paper published in 2019 IEEE Electric Ship Technologies Symposium - ESTS 2019
DOI: 10.1109/ESTS.2019.8847932